Theoretical and Applied Fracture Mechanics 104 (2019) 102345

Contents lists available at ScienceDirect

Theoretical and Applied Fracture Mechanics

journal homepage: www.elsevier.com/locate/tafmec

Statistical size scaling of compressive strength of quasi-brittle materials incorporating specimen length-to-diameter ratio effect

Wei-Sheng Lei[a], Guian Qian[b,*], Zhishui Yu[c,*], Filippo Berto[d]

[a] Applied Materials, Inc., Bldg.81, M/S 81305, 974 East Arques Ave., Sunnyvale, CA 94085, USA[1]
[b] State Key Laboratory of Nonlinear Mechanics (LNM), Institute of Mechanics, Chinese Academy of Sciences, Beijing 100190, China
[c] School of Materials Engineering, Shanghai University of Engineering Science, 333 Long Teng Rd., Shanghai 201620, China
[d] Department of Mechanical and Industrial Engineering, Norwegian University of Science and Technology (NTNU), Richard Birkelands vei 2b, 7491 Trondheim, Norway

ARTICLE INFO

Keywords:
Unconfined compressive strength
Quasi-brittle materials
Statistical size scaling
Volume effect
Length-to-diameter ratio effect

ABSTRACT

Statistical size scaling of compressive strength of quasi-brittle materials demands to define a global stress parameter pertinent to the well accepted mechanism of shear stress induced fracture. The work proposes to adopt the resultant stress acting on the diagonal cross-section of a uniaxial compression specimen from one loading end to the other loading end in place of the conventional nominal compressive stress on two loading ends for statistical size scaling. As a result, the size effect on compressive strength is partitioned into specimen volume effect and specimen length-to-diameter ratio effect according to a recently developed formulation for the generalized weakest link statistics. This proposal is validated by three published data sets on the compressive strength of concrete, rock and four cohesive soils as preliminary case studies.

1. Introduction

This work concerns the statistical size scaling of compressive strength of quasi-brittle materials measured from specimens with different length to diameter aspect ratios. Size effect on the strength of brittle and quasi-brittle materials exists under either tensile or compressive loading. A quantitative characterization of the size effect is needed to transfer the strength data measured from laboratory small-sized specimens under relatively simple loading conditions into the design codes and safety regulations for full-scale engineering structures serviced under complex loading conditions. Both deterministic methods and statistical approaches have been pursued to understand the size effect [1–7]. In addition to the size effect, strength values measured from a group of nominally identical specimens under same loading conditions also vary randomly. The random variation of strength arises from the inherent stochastic distribution of defects in materials at the microscopic and mesoscopic scales in terms of their spatial location, orientation, geometrical shape and size. These defects are either pre-existing in materials or developed as a result of progressive damage localization during loading. The interplay between size dependence and random variation of brittle failure strength necessitates the adoption of statistical approaches to tackle both aspects for size scaling. While the weakest-link statistics has been commonly used for tensile strength characterization, its applicability to the analysis of compressive strength has not been well agreed. As examples, Chen et al. [5] conducted the Kolomogorove-Smirnov goodness-of-fit tests and validated the feasibility of the modified Weibull distribution to 300 compressive strength data of concrete cores with different length-to-diameter ratios. Lei demonstrated the applicability of weakest-link statistics to the size effect on compressive strength of coal [6] and ceramics [7]. Bazant [1], Weiss et al. [4], Bazant and Xiang [8], Bertalan et al. [9], and Vu et al. [10] claimed the failure of weakest-link statistics in compressive loadings. As Lei [6,7] pointed out, Weibull statistics is not equivalent to weakest link statistics. Instead, Weibull statistics is only a subset of weakest link statistics. Therefore, the unsuccessful applications of Weibull statistics in [1,4,8–10] to compressive failure are not in a position to justify the failure of weakest link statistics. To the authors's opinion, among many other aspects that need to be addressed, a proper representation of the compressive strength is essential in the study of statistical size scaling. Fig. 1 shows a cylindrical specimen of diameter D and length L under uniaxial compressive loading force F. The unconfined compressive strength of a material is measured by the nominal stress $\sigma = 4F/(\pi D^2)$ at fracture. This uniaxial compression test is most widely used for measuring the compressive strength and size effect of geotechnical materials such as concrete [5,10], ice [11], coal [12], rocks [13], and cohesive soils [14]. It raises two concerns: (1). The

* Corresponding authors.
E-mail addresses: qianguian@imech.ac.cn (G. Qian), Yu_Zhishui@163.com (Z. Yu), filippo.berto@ntnu.no (F. Berto).
[1] Current address.

https://doi.org/10.1016/j.tafmec.2019.102345
Received 2 June 2019; Received in revised form 5 August 2019; Accepted 3 September 2019
Available online 06 September 2019

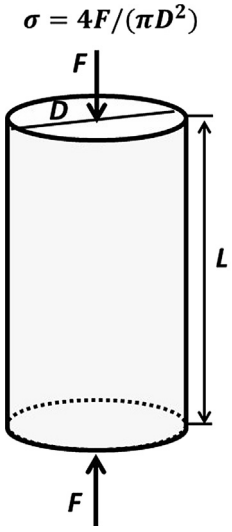

Fig. 1. A cylindrical specimen in unconfined uniaxial compression.

nominal compressive strength seems to work well for the case of proportional size scaling of strength, in which all specimens have a fixed value of length-to-diameter aspect ratio L/D while the magnitudes of L and D vary. However, does it also work for non-proportional size scaling of strength that involves specimens with different values of length-to-diameter aspect ratio L/D? (2). There lacks a sound justification or interpretation on how this nominal compressive strength σ is associated with the commonly accepted physical mechanism of shear stress induced failure for compressive loading. These two concerns motivate the present work to search for a proper representation of the compressive strength. The major purpose of this work is to propose and justify the adoption of the resultant stress σ_t acting on the diagonal cross-section of a uniaxial compression specimen from one loading end to the other loading end for statistical size scaling, followed by preliminary validation using some published data sets. The statistical size scaling will be based on a recently proposed generalized weakest-link statistical formulation [6], which will be briefly introduced first to facilitate the description.

2. Theoretical considerations

2.1. Introduction to the generalized weakest-link statistical formulation

The random distribution of various defects such as microcracks in a material can be characterized by four attributes namely, their spatial location, orientation, geometrical shape and size. Note that due to the difficulty in formulating the fracture probability induced by an individual defect that interacts with other defects, the assumption of mutual independence of defects is needed to develop the weakest-link formulation. However, these defects are not limited to preexisting ones. They can be developed due to progressive damage accumulation during the loading history, so long as they can cause unstable propagation or growth to incur fracture. Lei [6] proposed the generalized weakest-link formulation for brittle fracture induced by a population of mutually independent microcracks as follows:

$$P = 1 - \exp\left\{\int_V \ ln[1 - p(\sigma, V_0)]\cdot\frac{\partial N(V)}{\partial V}\cdot\delta V\right\} \tag{1}$$

where $N = N(V)$ is the number of microcracks in a volume V, which describes the spatial distribution of microcracks, or more generically, defects of sizes up to lateral size of an elemental volume V_0; $p(\sigma, V_0)$ is the probability for an existing microcrack of size a in the elemental volume V_o to propagate unstably under stress σ,

$$p(\sigma, V_0) = \int_{\sigma_{th}}^{\sigma_{eq,max}} F(\sigma_{eq} \geq S)\cdot g(S)\cdot dS \tag{2}$$

where σ_{th} is the threshold of fracture strength S, σ_{eq} is the effective stress acting on a volume element V_O, σ_{eq} is a function of principal stresses ($\sigma_1 \geq \sigma_2 \geq \sigma_3$), $\sigma_{eq,\max}$ is the upper bound value of σ_{eq}, $\sigma_{eq} = \sigma \geq S$ refers to the stress-based microscopic fracture criterion, which states that unstable fracture occurs when σ_{eq} reaches the critical strength S of a volume element V_0 embedded with a microcrack of size a. Different expressions of the effective stress σ_{eq} have been proposed [15]. $F(\sigma_{eq} \geq S)$ is the fracture probability of an existing microcrack, which depends on microcrack orientation and stress state, $g(S)$ is the probability density function (*PDF*) with respect to the fracture strength (S) of elemental volume V_O.

Under the simplest maximum *tensile* principal stress criterion,

$$\sigma_{eq} = \sigma_1 \geq S \tag{3}$$

there is

$$F(\sigma_1 \geq S) = \begin{cases} 1 & (\sigma_1 > 0) \\ 0 & (\sigma_1 \leq 0) \end{cases} \tag{4}$$

In turn, Eq. (2) reduces to the simplest format:

$$p(\sigma, V_0) = \int_{\sigma_{th}}^{\sigma_1} g(S)\cdot dS \tag{5}$$

Conceptually, the strength distribution *g(S)* is determined by microcrack size a and shape η, due to the Griffith law:

$$S = \sqrt{\frac{\eta E\gamma}{(1-\nu^2)a}} \tag{6}$$

where γ is the effective surface energy, E is the Young's modulus and ν is the Poisson's ratio. In real materials such as concrete, crack-type defects can be three-dimensional, such as those formed along the curved interfaces between reinforcement phases and matrix. So the accurate representation of defect shape factor distribution or even defect size distribution is very challenging. This is a major consideration to adopt strength distribution *g(S)* to represent the combined contributions of defect size and shape in Eq. (2).

Therefore, Eq. (1) collectively represents the combined effects of the four attributes of defects (spatial location, orientation, geometrical shape and size) and stress states in a material, as illustratively highlighted in Fig. 2.

By assuming a power-law function for the number of defects in a volume V,

$$N = N(V) = \left(\frac{V}{V_0}\right)^{\beta} \qquad (\beta > 0) \tag{7}$$

Eq. (1) reduces to

$$P = 1 - \exp\left\{\beta\left(\frac{V}{V_0}\right)^{\beta-1}\int_V \ ln[1 - p(\sigma, V_0)]\cdot\frac{\delta V}{V_0}\right\} \tag{8}$$

Note that $\beta > 0$ includes three scenarios, namely $\beta = 1$, $0 < \beta < 1$, $\beta > 1$ [6,7,16,17].

Next, under the maximum *tensile* principal stress criterion in Eq. (3), when *g(S)* is described by

$$g(S) = \frac{m}{\sigma_0}\left(\frac{S-\sigma_{th}}{\sigma_0}\right)^{m-1}\cdot\exp\left[-\left(\frac{S-\sigma_{th}}{\sigma_0}\right)^{m}\right] \qquad (\sigma_{th} \leq S < \infty) \tag{9}$$

Eq. (5) reduces to

$$p(\sigma, V_0) = 1 - exp\left[-\left(\frac{\sigma-\sigma_{th}}{\sigma_0}\right)^{m}\right] \qquad (\sigma_{th} \leq \sigma < \infty) \tag{10}$$

Consequently, Eq. (8) reduces to

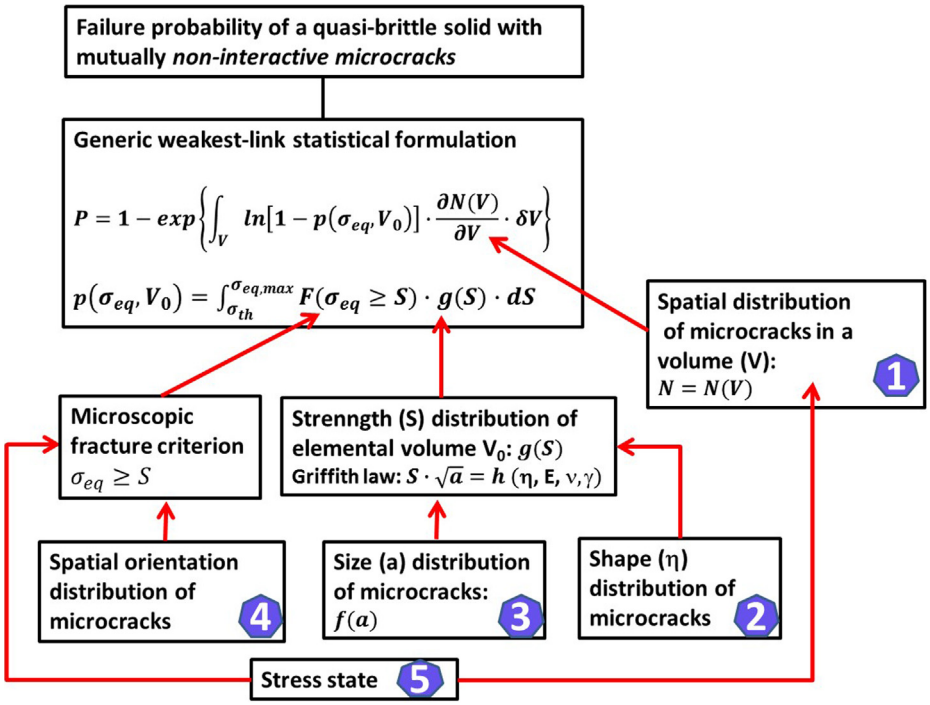

Fig. 2. Illustration of the combined effects of stress state and four microcrack attributes (spatial location, orientation, size and shape) on the cumulative failure probability.

$$P = 1 - exp\left[-\beta\left(\frac{V}{V_0}\right)^{\beta-1}\int_V \left(\frac{\sigma - \sigma_{th}}{\sigma_0}\right)^m \frac{\delta V}{V_0}\right] \quad (\sigma_{th} \leq \sigma < \infty) \tag{11}$$

Under uniform stress states such as uniaxial loading, Eq. (11) reduces to

$$P = 1 - exp\left[-\beta\left(\frac{\sigma - \sigma_{th}}{\sigma_0}\right)^m \left(\frac{V}{V_0}\right)^{\beta}\right] \quad (\sigma_{th} \leq \sigma < \infty) \tag{12}$$

When $\beta = 1$, the crack-type defects are uniformly distributed within a material, Eqs. (11) and (12) reduce to the three-parameter Weibull statistics,

$$P = 1 - \exp\left\{-\int_V \left(\frac{\sigma - \sigma_{th}}{\sigma_0}\right)^m \frac{\delta V}{V_0}\right\} \overset{uniform\sigma}{\Rightarrow} = 1 - exp\left[-\left(\frac{\sigma - \sigma_{th}}{\sigma_0}\right)^m \frac{V}{V_0}\right] (\sigma_{th} \leq \sigma < \infty) \tag{13}$$

In a real material, the exact PDFs of strength ($g(S)$) and defect orientation are unknown. More likely, defect orientation takes a non-uniform distribution. This makes it very challenging to pursue an analytical solution to $p(\sigma, V_0)$ in Eq. (2). As a result, an explicit expression of the cumulative failure probability P in terms of stress state, microcrack orientation, microscopic strength distribution $g(S)$ is rarely available. Alternatively, according to the first mean value theorem for integrals, Eq. (8) is rewritten as

$$\frac{1}{\beta V^{\beta}} \cdot \ln\left[\frac{1}{(1-P)}\right] = \frac{1}{V_0^{\beta}} \cdot \ln\left[\frac{1}{1 - p(\tilde{\sigma}, V_0)}\right] = \frac{h(\sigma_N)}{V_0^{\beta}} \tag{14}$$

where $\tilde{\sigma}$ is a stress value in the range $\sigma_{th} \leq \tilde{\sigma} \leq \sigma_N$, $h(\sigma_N)$ is a function of the nominal fracture strength σ_N.

Eq. (14) suggests a practical method to scaling size effect on strength by correlating the compound parameter $\frac{1}{\beta V^{\beta}} \cdot \ln\left[\frac{1}{(1-P)}\right]$ and nominal strength σ_N of different-sized specimens. It was validated by proportional size scaling of the strength of wood, concrete, gamma titanium aluminum alloy, nuclear-grade graphite, and aluminum foam in tension and coal in compression [6,7,17].

2.2. Selection of characteristic strength parameters for compressive failure size scaling

In addition to the four attributes of microcracks or defects, the roles of stress state in a material need to be emphasized. As highlighted in Fig. 2, stress state has an impact on the spatial distribution of microcracks, since during the loading history, progressive damage accumulation induces growth of preexisting microcracks until their unstable propagation is triggered to incur brittle failure. Furthermore, stress state also has an impact on the selection of appropriate microscopic fracture criterion $\sigma_{eq} \geq S$. Obviously, the commonly adopted maximum *tensile* principal stress criterion $\sigma_{eq} = \sigma_1 \geq S$ in tensile stress dominated loading conditions is no longer valid in compressive loading conditions such as uniaxial compression. Fig. 3a shows the cross section of a cylindrical or prismatic specimen with its two end faces subjected to uniaxial compression. The specimen height is denoted as L. The diameter of the end face is denoted as D. The volume element at an arbitrary material point M in the specimen is highlighted, in which a randomly oriented microcrack is embedded. Due to the remotely loaded global compressive stress σ, both a shear stress component τ' and a compressive normal stress component σ_n' are applied on the crack surface with its normal in an angle of α to the global compressive stress σ. On the one hand, microscopically, the Coulomb criterion is commonly adopted for the onset of brittle fracture under a compressive stress state as below,

$$\sigma_{eq} = |\tau'| + \mu \cdot \sigma_n' \geq S \tag{15}$$

where the sign convention of the normal stress component σ_n is positive in tension and negative in compression, μ is an internal friction coefficient, S now refers to the cohesion strength. Due to material heterogeneity and the random microcrack orientation, both μ and S are random variables. On the other hand, as mentioned in Section 1. Introduction, the peak value of the global compressive stress σ is conventionally taken as the nominal compressive strength and is also directly adopted for statistical analysis. As shown in Fig. 3a, there is

$$\sigma_n' = \sigma \cdot cos^2\alpha, \ \tau' = \sigma sin\alpha \cdot cos\alpha \tag{16}$$

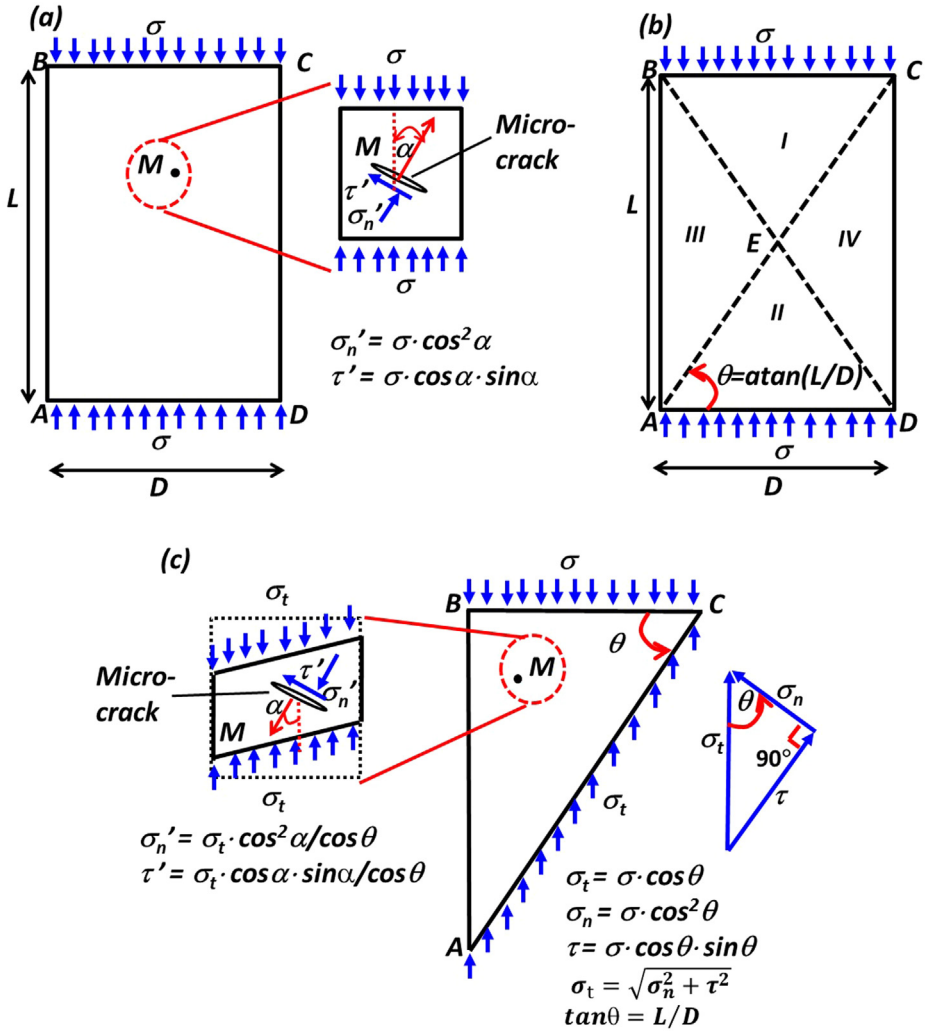

Fig. 3. Characteristic strength parameters for compressive failure analysis: Cross-sectional view of a specimen in uniaxial compression and a volume element embedded with a microcrack in point M (a); four zones of the specimen defined by the end-to-end diagonal cross sections $\bar{AC}$ and $\bar{BD}$ (b); stress analysis along the cross section $\bar{AC}$ and a volume element embedded with a microcrack in point M (c).

Eq. (15) is rewritten as

$$\sigma_{eq} = \sigma \cdot cos\alpha \cdot (cos\alpha + \mu \cdot sin\alpha) \geq S \tag{17}$$

Regardless of the complexity of the solution to $p(\sigma, V_0)$ in Eq. (2) due to the unknown distributions of microcrack orientation angle α and the internal friction coefficient μ, the formulation (17) suggests that $p(\sigma, V_0)$ relates to the nominal compressive strength σ. From this aspect, the adoption of nominal compressive strength σ in engineering seems to be in line with the Coulomb criterion in Eq. (15). However, one major problem is that this nominal compressive strength σ is incapable of manifesting the impact of specimen aspect ratio (L/D) on the onset of failure. It is thus necessary to look for a better stress parameter that can also reflect the effect of specimen aspect ratio (L/D). Now the specimen in Fig. 3a is equivalently represented in Fig. 3b, where the whole specimen is partitioned into four zones I, II, III, and IV by the two diagonal lines $\bar{AC}$ and $\bar{BD}$. Due to the symmetry of both loading and specimen geometry, for a macroscopically homogeneous material, zone I (ΔBEC) and zone II (ΔAED) have the identical mechanical performance, so do zone III (ΔAEB) and zone IV (ΔCED). The same stress state exists along the diagonal edges (lines $\bar{AC}$ and $\bar{BD}$). As shown in detail in Fig. 3c, the resultant stress σ_t on the two diagonal lines $\bar{AC}$ and $\bar{BD}$ is a function of the specimen aspect ratio (L/D) as follows:

$$tan\theta = L/D,\ cos\theta = 1/\sqrt{1 + (L/D)^2} \tag{18}$$

$$\sigma_t = \sigma \cdot cos\theta = \sigma/\sqrt{1 + (L/D)^2} \tag{19}$$

Accordingly, the shear stress component τ' and the normal stress component σ_n' acting on an arbitrary microcrack surface can be reformulated in terms of the resultant stress σ_t as below:

$$\sigma_n' = \sigma_t \cdot cos^2\alpha/cos\theta,\ \tau' = \sigma_t \cdot sin\alpha \cdot cos\alpha/cos\theta \tag{20}$$

Therefore, the resultant stress σ_t on the diagonal sections of the specimen embodies the effects of both the nominal compressive stress σ and the specimen aspect ratio (L/D). For a group of specimens with a fixed aspect ratio (L/D = constant), the angle θ remains unchanged. The case reduces to proportional size scaling, and there is no difference of using either σ_t or σ. However, when specimens of different aspect ratios (L/D) are involved, the adoption of the resultant stress σ_t has a clear merit over that of σ. Therefore, in Eq. (14), we now propose to use $\sigma_N = \sigma_t$ instead of $\sigma_N = \sigma$ as the nominal strength to investigate the correlation between the compound parameter $\frac{1}{\beta V^{\beta}} \cdot \ln\left[\frac{1}{(1-P)}\right]$ and σ_t in Eq. (19) for size scaling of compressive strength of specimens of different length-to-diameter ratios. As a preliminary effort, Section 3 is dedicated to the case studies of three published data sets to validate this proposal.

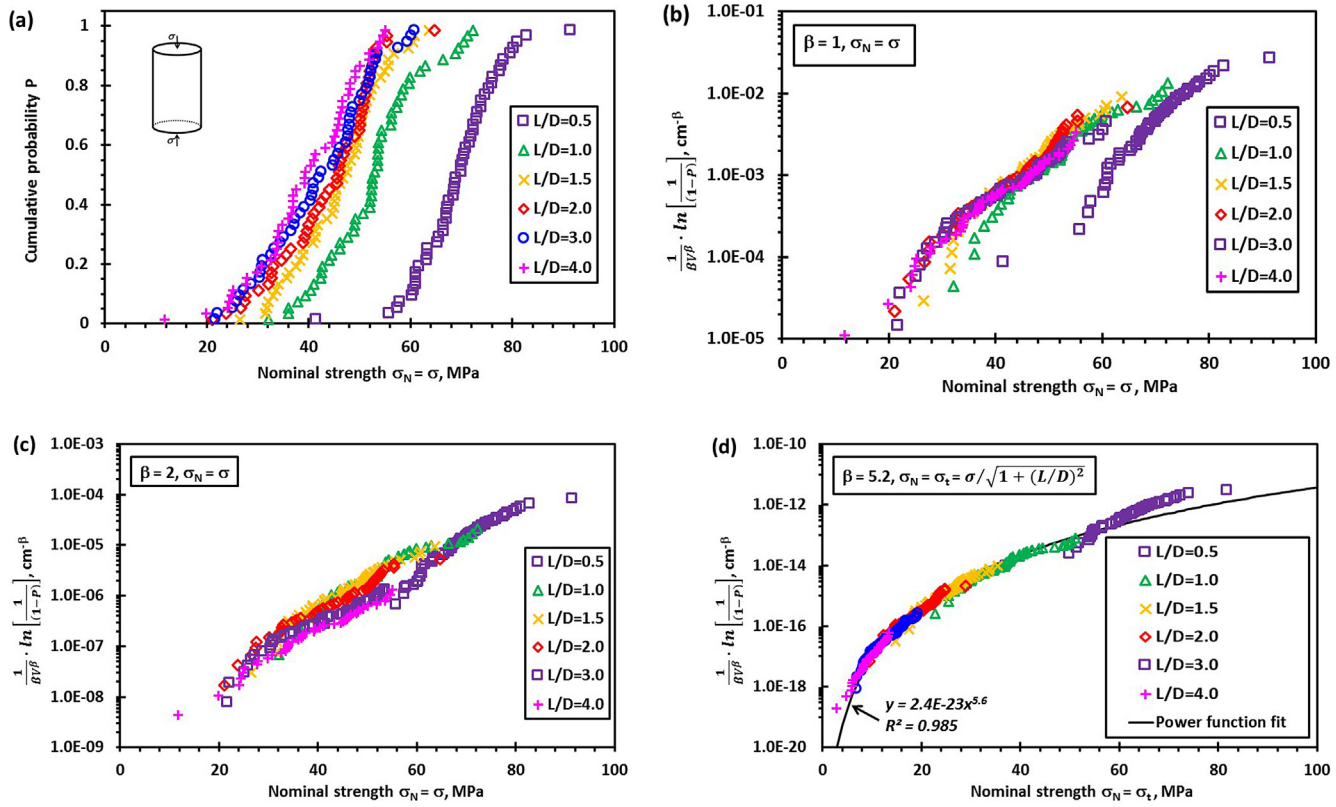

Fig. 4. Compressive strength of 74 mm diameter concrete cores with different lengths: raw strength (σ) data [4] (a); correlation between $\frac{1}{V}\cdot\ln\left[\frac{1}{(1-P)}\right]$ and $\sigma_N = \sigma$ (b); correlation between $\frac{1}{\beta V^{\beta}}\cdot\ln\left[\frac{1}{(1-P)}\right]$ and $\sigma_N = \sigma$ (c); correlation between $\frac{1}{\beta V^{\beta}}\cdot\ln\left[\frac{1}{(1-P)}\right]$ and $\sigma_N = \sigma_t$ (d).

3. Case studies

3.1. Compressive strength of concrete cores with different length-to-diameter ratios

Chen et al. [5] studied the statistical distribution of compressive strength of concrete cores with a fixed diameter (D) of 74 mm but different length-to-diameter (L/D) ratios of 0.5, 1.0, 1.5, 2.0, 3.0, and 4.0. The maximum aggregate size is 20 mm. At each aspect ratio (L/D), 50 core specimens were tested. In total, 300 strength data were reported in a tabular form, and are shown here in Fig. 4a. The 50 strength data points in each group are arranged in an ascending order. Then the rank probability for the i-th strength datum is given by:

$$P_i = \frac{i - 0.3}{n + 0.4} \quad (i = 1, 2, \cdots, n;\ n = 50) \tag{21}$$

The strength data at each aspect ratio (L/D) were fit with the following modified Weibull distribution to account for the length (L) effect in [5]:

$$\mathrm{P} = 1 - \exp\left[-\left(\frac{L}{L_0}\right)^{\beta}\left(\frac{\sigma}{\sigma_0}\right)^{m}\right] \tag{22}$$

Their fitting results are reported in Table 1. While β has a fixed value of 3.848, both the estimated values of m and σ_0 vary with the aspect ratio (L/D).

Now Eq. (14) is adopted to seek the correlation between $\frac{1}{\beta V^{\beta}}\cdot\ln\left[\frac{1}{(1-P)}\right]$ and the nominal strength σ_N in two ways. First, the remote compressive strength σ is taken as the nominal strength, $\sigma_N = \sigma$. This leads to a poor correlation for either $\beta = 1$ (uniform spatial distribution of defects) or $\beta \neq 1$ (non-uniform spatial distribution of defects) as shown in Fig. 4b and Fig. 4c, respectively. Second, the resultant stress on the diagonal sections σ_t given in Eq. (19) is taken as the nominal strength, $\sigma_N = \sigma_t = \sigma/\sqrt{1 + (L/D)^2}$. All the data fall on a master curve with $\beta = 5.2$ (non-uniform spatial distribution of defects) as shown in Fig. 4d. This example clearly demonstrates the merit of adopting the resultant stress σ_t in place of the conventional nominal stress σ for statistical analysis of size effect on uniaxial compressive strength. This master curve correlating $\frac{1}{\beta V^{\beta}}\cdot\ln\left[\frac{1}{(1-P)}\right]$ and σ_t is fitted by a power function ($y = ax^m$) with the coefficient of determination $R^2 = 0.985$ as shown in Fig. 4d. In equivalence, the power function fit is given as below:

$$P = 1 - exp\left[-\beta\left(\frac{\sigma}{\sigma_0\sqrt{1 + (L/D)^2}}\right)^{m}\left(\frac{V}{V_0}\right)^{\beta}\right] \tag{23}$$

with $\beta = 5.2$, m = 5.6, $\sigma_0 = 10945.8MPa$, $V_0 = 1cm^3$, $V = \pi LD^2/4$, $R^2 = 0.985$.

While the uniqueness of the master curve correlation between $\frac{1}{\beta V^{\beta}}\cdot\ln\left[\frac{1}{(1-P)}\right]$ and σ_t is convincing, we admit that the relatively power function does not accurately represent all the data points.

Table 1
Estimation of Weibull parameters of concrete compressive strength data [4].

L/D	Ref. [4] Eq. (23)				This study Eq. (24)			
	m	σ_0, MPa	β	R^2	m	σ_0, GPa	β	R^2
0.5	8.491	59.815	3.848	0.945	5.6	10.95	5.2	0.985
1.0	6.960	57.122		0.981				
1.5	6.557	63.328		0.985				
2.0	4.947	80.566		0.982				
3.0	4.446	116.801		0.977				
4.0	3.999	164.863		0.968				

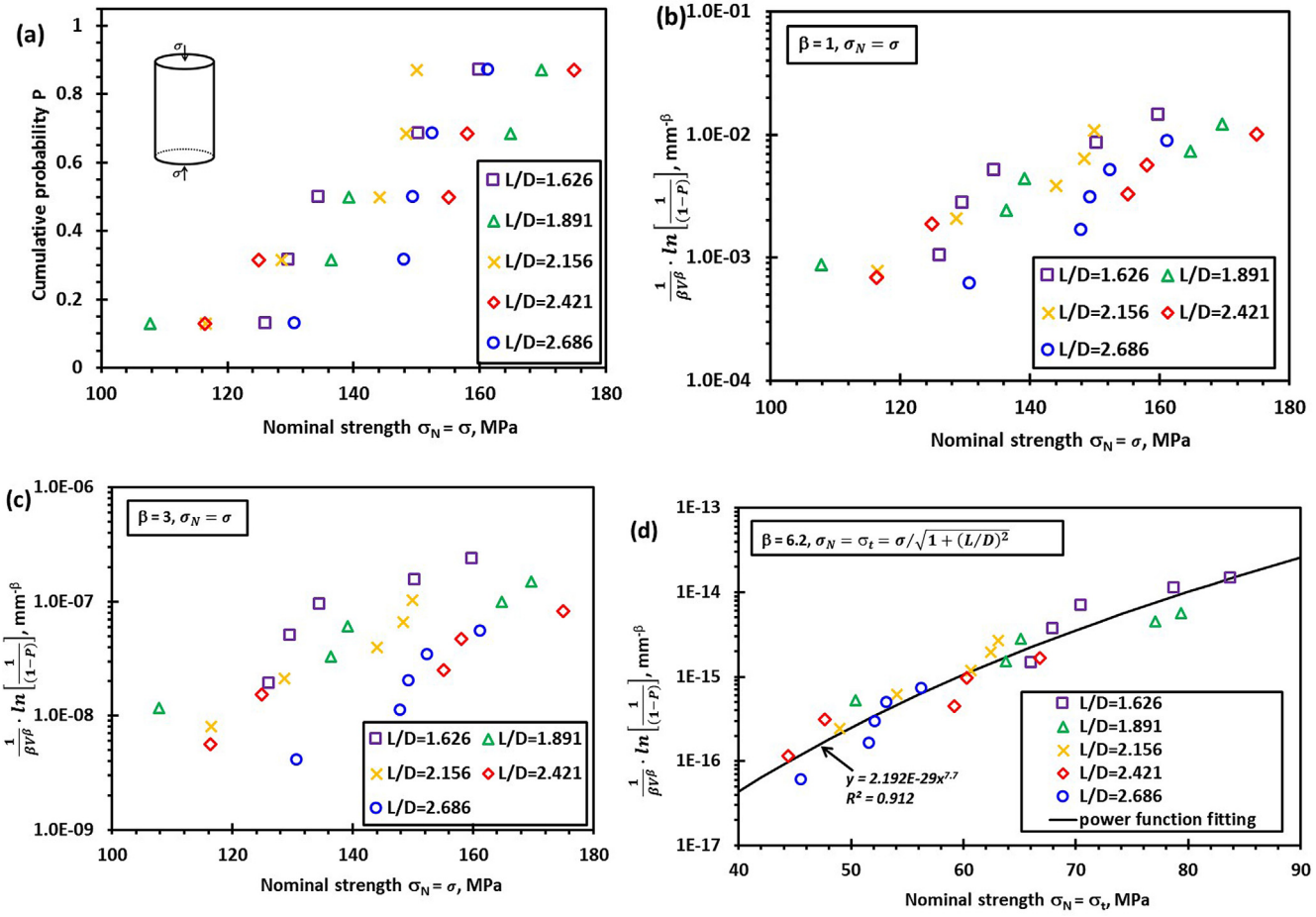

Fig. 5. Compressive strength of 47.5 mm diameter rock with different lengths: raw strength (σ) data [13] (a); correlation between $\frac{1}{V}\cdot\ln\left[\frac{1}{(1-P)}\right]$ and $\sigma_N = \sigma$ (b); correlation between $\frac{1}{\beta V^{\beta}}\cdot\ln\left[\frac{1}{(1-P)}\right]$ and $\sigma_N = \sigma$ (c); correlation between $\frac{1}{\beta V^{\beta}}\cdot\ln\left[\frac{1}{(1-P)}\right]$ and $\sigma_N = \sigma_t$ (d).

3.2. Compressive strength of rock specimens with different length-to-diameter ratios

Li et al. [13] studied the statistical distribution of compressive strength of cylindrical rock specimens with a fixed diameter of 47.5 mm but different length-to-diameter (L/D) ratios of 1.60, 1.87, 2.14, 2.41, and 2.67 as actual measurement (the target L/D ratios being 1.5, 1.75, 2.0, 2.25, 2.5). At each aspect ratio (L/D), only 5 specimens were tested. The strength data were given in tabular format and are plotted in Fig. 5a. Now Eq. (14) is adopted to seek the correlation between $\frac{1}{\beta V^{\beta}}\cdot\ln\left[\frac{1}{(1-P)}\right]$ and the conventional nominal strength, $\sigma_N = \sigma$. This leads to a poor correlation for either $\beta = 1$ (uniform spatial distribution of defects) or $\beta \neq 1$ (non-uniform spatial distribution of defects) as shown in Fig. 5b and c, respectively. Now we seek the correlation between $\frac{1}{\beta V^{\beta}}\cdot\ln\left[\frac{1}{(1-P)}\right]$ and the nominal strength $\sigma_N = \sigma_t = \sigma/\sqrt{1+(L/D)^2}$. As shown in Fig. 5d, all the data sit on a master curve defined by Eq. (24),with $\beta = 6.2$, m = 7.7, $\sigma_0 = 5331$ MPa, $V_0 = 1$ cm^3, $V = \pi LD^2/4$, $R^2 = 0.912$. The small number of specimens (5) in each group should be responsible for the relatively large scatter of strength data in Fig. 5a and d.

3.3. Compressive strength of cohesive soil specimens with different length to diameter aspect ratios

Güneyli and Rüsen [14] studied the effect of length-to-diameter ratio on the unconfined compressive strength of cohesive soil specimens. Four soil materials were tested namely, Handere clay, Alamanpinari clay, Sam-Tekin clay, and kaolinate. The samples for unconfined compression testing were prepared with the optimum moisture content to eliminate the effects of the moisture content, void ratio, and natural density on the unconfined compressive strength. Each soil sample was first oven-dried at 60 °C, then it was compacted using a standard Proctor mold at the optimum moisture content and the maximum dry density according to the compaction curves. Next, a thin-walled stainless steel sampling tube with an inner diameter of 48 mm, a length of 19 cm, and a wall thickness of 1.5 mm was driven into the soil in the standard Proctor mold with a hydraulic jack to immediately extrude the soil from the sampling tube by another hydraulic jack and its ends were cut to make it the desired length. The inner surface of the sampling tube was lightly lubricated to minimize the side friction, which can damage soil samples during intrusion and extrusion. The weight of each sample was measured to an accuracy of about 0.01 g and then wrapped in plastic foil to avoid significant variations in water content. The samples isolated in this way were kept under ambient conditions at 24 ± 2 °C for seven days in order to ensure moisture uniformity. Cylindrical specimens were prepared for each soil material with a fixed diameter (D) of 48 mm and 11 different length-to-diameter (L/D) ratios (from 0.5:1 to 3:1), corresponding to lengths from 24 to 144 mm. The average values of the compressive strength along with the standard deviations were reported as presented in Table 2, while the individual strength measurement for each specimen was not given. Therefore, we need to first formulate the mean value of strength as a function of the aspect ratio based on Eq. (23).

Eq. (23) is equivalent to

Table 2
Uniaxial compressive strength data of cohesive soils [14].

L/D ratio	Average strength ($\bar{\sigma}$) ± standard deviation (δ_σ), MPa			
	Sam-Tekin clay	Kaolinite	Handere clay	Almanpinari clay
0.50	3.4663 ± 0.067	2.2866 ± 0.087	1.9947 ± 0.074	4.2623 ± 0.182
0.75	3.2865 ± 0.065	1.9479 ± 0.101	1.7606 ± 0.060	3.9573 ± 0.171
1.00	3.0110 ± 0.068	1.6949 ± 0.096	1.2222 ± 0.099	3.8475 ± 0.176
1.25	2.5814 ± 0.149	1.6724 ± 0.097	1.1480 ± 0.113	3.3142 ± 0.243
1.50	2.4942 ± 0.167	1.5230 ± 0.122	1.0509 ± 0.124	3.1045 ± 0.251
1.75	2.2791 ± 0.180	1.4148 ± 0.123	0.9860 ± 0.132	2.9289 ± 0.212
2.00	2.1980 ± 0.216	1.3327 ± 0.126	0.9130 ± 0.142	2.6190 ± 0.224
2.25	2.1826 ± 0.211	1.2405 ± 0.145	0.8836 ± 0.170	2.5085 ± 0.264
2.50	2.0770 ± 0.225	1.0882 ± 0.144	0.8761 ± 0.157	2.4229 ± 0.291
2.75	2.0090 ± 0.266	0.6928 ± 0.208	0.7786 ± 0.218	1.8662 ± 0.446
3.00	1.8760 ± 0.297	0.6330 ± 0.229	0.7404 ± 0.267	1.8630 ± 0.479

$$P = 1 - exp\left[-\left(\frac{\sigma}{\sigma_u}\right)^m\right] \tag{24}$$

With

$$\sigma_u = \frac{\sigma_0}{\sqrt[m]{\beta}}\sqrt{1+(L/D)^2}\cdot\left(\frac{V_0}{V}\right)^{\frac{\beta}{m}} \tag{25}$$

Therefore, the mean value of strength σ is

$$\bar{\sigma} = \sigma_u\cdot\Gamma\left(1+\frac{1}{m}\right) = \frac{\sigma_0}{\sqrt[m]{\beta}}\sqrt{1+(L/D)^2}\cdot\left(\frac{V_0}{V}\right)^{\frac{\beta}{m}}\cdot\Gamma\left(1+\frac{1}{m}\right) \tag{26}$$

Eq. (26) is rewritten as:

$$\frac{\bar{\sigma}}{\sqrt{1+(L/D)^2}} = \frac{\sigma_0}{\sqrt[m]{\beta}}\cdot\left(\frac{V_0}{V}\right)^{\frac{\beta}{m}}\cdot\Gamma\left(1+\frac{1}{m}\right) \tag{27}$$

Since the diameter (D) has a fixed value (48 mm) for all the specimens,

$$\mathrm{V} = \frac{\pi}{4}LD^2 = \frac{\pi D^3}{4}\cdot\left(\frac{L}{D}\right) \propto \frac{L}{D} \tag{28}$$

Eq. (27) is rewritten as

$$\frac{\bar{\sigma}}{\sqrt{1+(L/D)^2}} = \frac{C}{(L/D)^\eta} \tag{29}$$

Or

$$\bar{\sigma} = \frac{C\cdot\sqrt{1+(L/D)^2}}{(L/D)^\eta} \tag{30}$$

$$C = \frac{\sigma_0}{\sqrt[m]{\beta}}\cdot\left(\frac{4V_0}{\pi D^3}\right)^{\frac{\beta}{m}}\cdot\Gamma\left(1+\frac{1}{m}\right),\ \text{and}\ \eta = \frac{\beta}{m} > 0 \tag{31}$$

According to Eq. (29), we now seek the correlation between $\frac{\bar{\sigma}}{\sqrt{1+(L/D)^2}}$ and the aspect ratio L/D, as shown in Fig. 6a and b. For all the four soil materials, the power law correlation between $\frac{\bar{\sigma}}{\sqrt{1+(L/D)^2}}$ and L/D does exit, with $\eta = \frac{\beta}{m}$ = 0.96, 1.227, 1.152, 1.073 for Sam-Tekin clay, Kaolinite, Handere clay, and Almanpinari clay, respectively. With the information of statistical distribution of strength for each soil (which was not reported in [13]), the values of β and m can be further determined.

However, if we take the remote compressive strength σ s the nominal strength, $\sigma_N = \sigma$, while Eq. (24) is still valid, Eqs. (25) and (26) reduce to,

$$\sigma_u = \frac{\sigma_0}{\sqrt[m]{\beta}}\cdot\left(\frac{V_0}{V}\right)^{\frac{\beta}{m}} \tag{32}$$

$$\bar{\sigma} = \sigma_u\cdot\Gamma\left(1+\frac{1}{m}\right) = \frac{\sigma_0}{\sqrt[m]{\beta}}\cdot\left(\frac{V_0}{V}\right)^{\frac{\beta}{m}}\cdot\Gamma\left(1+\frac{1}{m}\right) \tag{33}$$

Due to Eq. (28) for a fixed value of D, Eq. (33) is rewritten as

$$\bar{\sigma} = \frac{C}{(L/D)^\eta} \tag{34}$$

Fig. 6c and d show the correlation between $\bar{\sigma}$ and L/D. A comparison of the values of coefficient of determination R^2 for each same material supports to correlate $\frac{\bar{\sigma}}{\sqrt{1+(L/D)^2}}$ instead of $\bar{\sigma}$ with the aspect ratio L/D.

4. Discussions

The difference in size effect on brittle fracture induced by tension and by compression is an interesting point to discuss. First, the size effect on strength is well understood for tensile loading induced failure. It essentially reduces to specimen volume effect for a given tensile loading mode [16]. However, for compressive loading induced failure, as revealed in Eq. (27), there are two aspects of the size effects on the mean value of strength $\bar{\sigma}$, namely the volume effect and the length-to-diameter ratio effect. Conceptually, Eq. (27) suggests that the mean value of unconfined compressive strength $\bar{\sigma}$ is a function of material structural properties (Weibull modulus m, scale parameter σ_0, elemental volume V_0, and defect spatial distribution parameter β) and specimen geometries (volume V and length-to-diameter ratio L/D) as follows:

$$\bar{\sigma} = f(V_0, \sigma_0, m, \beta, V, L/D) \tag{35}$$

Second, for the spatial distribution of defects in quasi-brittle materials under tensile loading, $0 < \beta \leq 1$ is found (e.g. $\beta = 1$ for concrete) in [6,16], while under compressive loading, both $0 < \beta \leq 1$ (e.g. $\beta = 0.5$ for coal in [6]) and $\beta > 1$ (for concrete and rock in this study) are found. It would be interesting to conduct tensile tests and compressive tests respectively on a same material (e.g. concrete) and compare the values of β inferred from both tests. If they are significantly different, it will validate the argument that both the preexisting defects and those developed due to progressive damage accumulation during loading process contribute to the final unstable failure event.

While these three case studies support the proposed idea, more experimental data will be needed for validation before it is adopted for engineering practice. Particularly, these three case studies all designed specimens of different aspect ratio (L/D) by fixing specimen diameter D and varying specimen length L. This method of experimental design may be due to practical demand in their engineering applications. In order to validate this model, we do need strength data from specimens of different aspect ratio (L/D) by varying D while fixing L or by varying both D and L in future studies. However, since in the model, the parameters V_0, σ_0, m, β are assumed material properties, so long as the

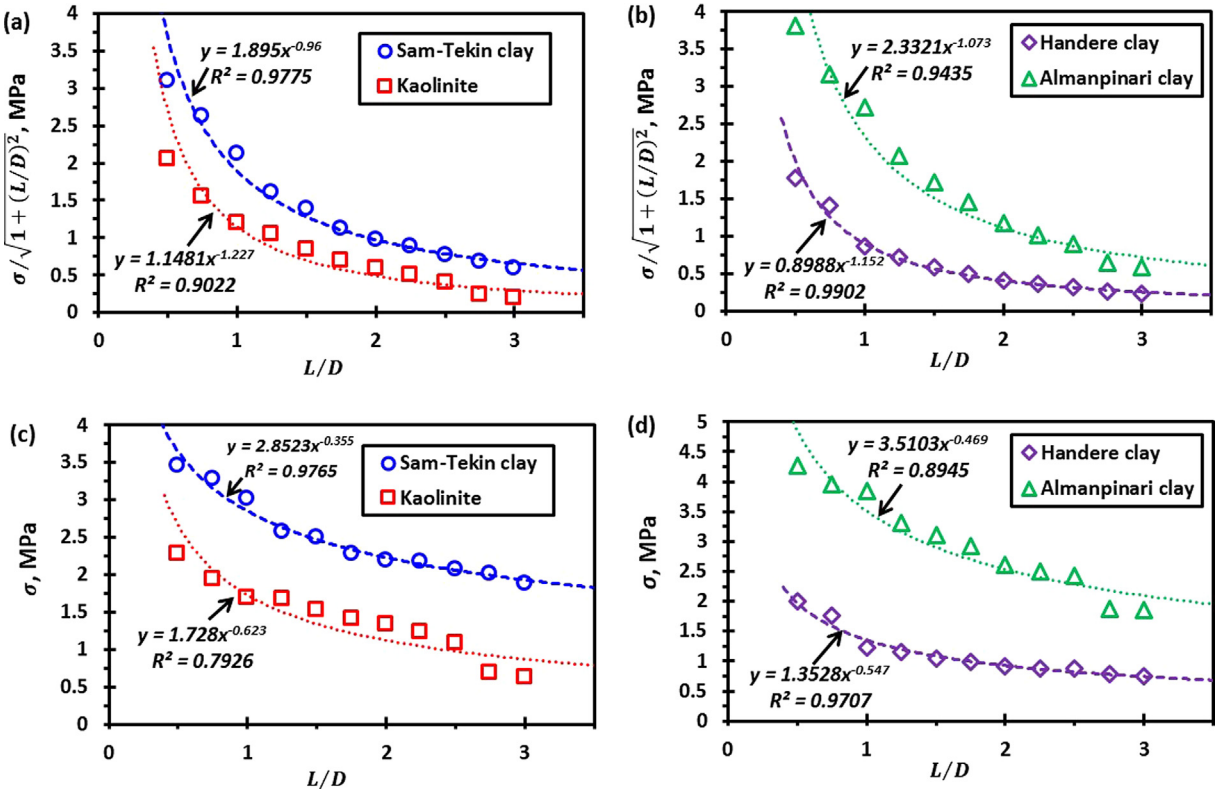

Fig. 6. Correlation between $\sigma_t = \sigma/\sqrt{1+(L/D)^2}$ and length-to-diameter (L/D) ratio of four soils, namely Same-Tekin clay and Kaolinite (a), and Handere clay and Alamanpinari clay (b) according to Eq. (29), in comparison with Correlation between σ and length-to-diameter (L/D) ratio (c) and (d).

specific preparation method of specimens with different aspect ratio (L/D) by varying either L or D or both does not cause change of these material properties, the proposed model is expected to still hold.

The relationship between Weibull statistics and weakest link statistics is explained in Section 1. Introduction. In brief, since Weibull statistics is only a subset of weakest link statistics, the failure of Weibull statistics in [1,4,8–10] to compressive failure are insufficient to reject weakest link statistics for compressive failure analysis. The reader is cautioned to distinguish between Weibull distribution function and Weibull statistical analysis for failure of materials. Specifically, Eq. (9) is the so-called Weibull distribution function, which is the PDF for strength of an elemental volume V_0, Eq. (10) is the fracture probability of an elemental volume V_0 under stress σ. While Weibull statistical analysis for failure of materials refers to the combination of weakest link statistics for a bulk material of volume V and the Weibull distribution function in Eq. (9) for the strength of an elemental volume V_0, which leads to Eq. (13), under the assumption of uniform spatial distribution of flaws. As shown in Figs. 4b and 5b, the failure of using Eq. (13) to describe statistical characteristics of compressive strength only concludes the incompetence of Weibull statistical analysis for compressive strength, and is insufficient to claim the failure of weakest link statistics. Note that Eq. (12) is not a Weibull model of strength. Eq. (12) is a weakest link model with the specific assumption of strength of elemental volume V0 in Eq. (9) and the power-law function for the number of defects in a volume V. The successful application of Eq. (12) in characterizing the statistics of compressive strength in Figs. 4d, 5d, and 6a,b validates the applicability of weakest link statistics in compressive strength analysis.

When the weakest link postulate is applied to failure analysis of a solid of volume V subjected to arbitrary multi-axial stresses, its total volume (V) is divided into many small volume elements, each of which is subjected to a quasi-homogeneous stress state and may contain certain number of elemental volume V_0. These small volumes are conceptually assumed to be linked in series. The failure of each small volume element is assumed an independent event. When the failure probability of an elemental volume V_0, $p(\sigma, V_0)$, is known, the weakest link model for the cumulative failure probability of the whole solid is obtained in Eq. (1). In a nutshell, this methodology combines weakest link analysis and micromechanics. The contribution of micromechanics is manifested by $N = N(V)$, the number of flaws in a volume V, in Eq. (1). Note that in the presentation, the terms “microcrack” and “defect” are used interchangeably in the presentation. Strictly, the term “defect” is more appropriate than “microcrack” to describe a flaw in a material, as its size is unnecessarily at microscale, but can be as large as the lateral size of an elemental volume V_0, depending on the specific material being studied. Moreover, these defects can be initially pre-existing one as a result of material preparation before loading, or can be the instantaneous growing-up flaws at certain phase of loading, so long as they can cause unstable propagation to induce fracture. Note that due to the difficulty in formulating the fracture probability induced by an individual defect that interacts with other defects, the assumption of mutual independence of defects is needed to formulate the weakest-link model.

5. Conclusion

Since the conventional nominal compressive stress on the loading ends of a specimen is not sensitive enough to reflect the effect of specimen length to diameter ratio on uniaxial compressive strength, the resultant stress σ_t acting on the loading end-to-loading end diagonal cross-section of a cylindrical specimen in uniaxial compression is proposed to replace the conventional nominal compressive stress for statistical size scaling of compressive strength of quasi-brittle materials when specimens of different length to diameter ratios are involved. This proposal is validated by three case studies of published strength data sets from specimens of different length to aspect ratios by changing specimen length only while fixing specimen diameter.

Declaration of Competing Interest

The authors declare that there is no conflict of interest.

Acknowledgement

Guian Qian thanks to the National Natural Science Foundation of China (No. 11872364) and Chinese Academy of Science (CAS) Pioneer Hundred Talents Program for funding the research.

Appendix A. Supplementary material

Supplementary data to this article can be found online at https://doi.org/10.1016/j.tafmec.2019.102345.

References

[1] Z.P. Bazant, Scaling theory for quasibrittle structural failure, Proc. Natl. Acad. Sci. (PNAS) USA 101 (2004) 13400–13407.
[2] A. Carpinteri, B. Chiaia, P. Cornetti, On the mechanics of quasi-brittle materials with a fractal microstructure, Eng. Fract. Mech. 70 (2003) 2321–2349.
[3] B.L. Karihaloo, H.M. Abhalla, Q.Z. Xiao, Deterministic size effect in the strength of cracked concrete structures, Cem. Concr. Res. 36 (2006) 171–188.
[4] J. Weiss, L. Girard, F. Gimbert, D. Amitrano, D. Vandembroucq, (Finite) statistical size effects on compressive strength, Proc. Natl. Acad. Sci. 111 (17) (2014) 6231–6236, https://doi.org/10.1073/pnas.1403500111.
[5] X. Chen, S. Wu, J. Zhou, Compressive strength of concrete cores with different lengths, ASCE J. Mater. Civ. Eng. 26 (2014) 04014027-1–04014027-7.
[6] W.S. Lei, A generalized weakest-link model for size effect on strength of quasi-brittle materials, J. Mater. Sci. 53 (2018) 1227–1245.
[7] W.S. Lei, Statistical size scaling of ceramic strength, J. Am. Ceram. Soc. 102 (2018) 90–97.
[8] Z.P. Bazant, Y. Xiang, Size effect in compression failure: splitting crack band propagation, J. Eng. Mech. 123 (1997) 162–172.
[9] Z. Bertalan, A. Shekhawat, J.P. Sethna, S. Zapperi, Fracture strength: stress concentration, extreme value statistics, and the fate of the Weibull distribution, Phys. Rev. Appl. 2 (2014) 1–8.
[10] C.-C. Vu, J. Weiss, O. Plé, D. Amitrano, D. Vandembroucq, Revisiting statistical size effects on compressive failure of heterogeneous materials, with a special focus on concrete, J. Mech. Phys. Solids 121 (2018) 47–70.
[11] G.A. Kuehn, E.M. Schulson, D.E. Jones, J. Zhang, The compressive strength of ice cubes of different sizes, Trans. ASME J. Offshore Mech. Arctic Eng. 115 (1993) 142–148.
[12] C. Gonzatti, L. Zorzi, I.M. Agostini, J.A. Fiorentini, A.P. Viero, R.P. Philipp, In situ strength of coal bed based on the size effect study on the uniaxial compressive strength, Int. J. Min. Sci. Technol. 24 (2014) 747–754.
[13] X. Li, C. Liu, W. Guo, J. Qiu, The effect of specimen height on the uniaxial compressive experiment of rocks, Electr. J. Geotech. Eng. 20 (2015) 1473–1486. Available at http://www.ejge.com/2015/Ppr2015.0224mb.pdf.
[14] H. Güneyli, T. Rüsen, Effect of length-to-diameter ratio on the unconfined compressive strength of cohesive soil specimens, Bull. Eng. Geol. Environ. 75 (2016) 793–806.
[15] W.S. Lei, A cumulative failure probability model for cleavage fracture in ferritic steels, Mech. Mater. 93 (2016) 184–198.
[16] W.S. Lei, Z. Yu, A statistical approach to scaling size effect on strength of concrete incorporating spatial distribution of flaws, Build. Constr. Mater. 122 (2016) 702–713.
[17] G. Qian, W.S. Lei, Z. Yu, F. Berto, Statistical size scaling of breakage strength of irregularly-shaped particles, Theor. Appl. Fract. Mech. 102 (2019) 51–58.